

## Transonic Flow Simulation Around the plunging Airfoil with Oscillation of Flow Boundary Condition

M.H Djavareshkian and A.R. Faghihi

**Abstract**— A new pressure based implicit procedure to solve the Euler and Navier-Stokes equations is developed to predict transonic viscous and inviscid flows around the plunging airfoil with high resolution scheme. In this process, nonorthogonal and non moving mesh with collocated finite volume formulation are used. In order to simulate plunging airfoil, oscillation of flow boundary condition is applied. The boundedness criteria for this procedure are determined from Normalized Variable Diagram (NVD) scheme. The procedure incorporates the  $k-\varepsilon$  eddy-viscosity turbulence model. In the new algorithm, the computation time is considerably reduced. This process is tested for inviscid and turbulent transonic aerodynamic flows around plunging airfoil. The results are compared with other existing numerical solutions and with experiment data. The comparisons show that the resolution quality of the developed algorithm is considerable.

**Keywords**— Plunging, Transonic, Inviscid, Viscous, Boundary condition

### I. Introduction

In the field of simulating moving boundary flow problems, different approaches are found in the literature of the art. Shankar and Ide [1] have presented an appropriate grid update procedure for small displacements of the structure where the speeds of the outer boundary points are taken to be zero and the grid speeds at any interior point are then obtained by interpolating the body value and the zero outer boundary value along a constant coordinate line. However, this method may result in severe grid distortions when the structure experiences large displacements. Goswami and Parpia [2] mentioned that local grid restructuring methods can be used when at each time step, the boundary movement is smaller than the minimum mesh size in the domain. Regarding the high cost of mesh insertion and deletion in the previous method Batina [3] introduced dynamic mesh approach. This method uses mesh smoothing instead of insertion and deletion of near boundary grids. The process of Mesh smoothing is implemented until a proper mesh quality, which is dependent on several criteria is achieved [4]. In order to attain a pattern for grid points to satisfy a set of smoothness and orthogonality constraints, Nakahashi and Deiwert [5] used the concept of spring coupled with variation principles. Levine et al. [6] utilized the similar spring analogy to compute the new body conforming grid

points. Guruswamy [7] introduced a dynamic algebraic grid generation scheme in which grid points are conformed to the deforming shapes of the structure. Lohner [8] proposed the use of the Arbitrary Lagrangian-Eulerian (ALE) formulation as a means to achieve a solver that can handle moving frames. However the grid points in ALE formulation must be renewed even in the sheer rigid-body motion problems. Farhat and Lin [9] introduced a more economical approach for transient solution of the aeroelastic coupled problem with respect to multiple moving frames of reference.

Other approaches for handling moving boundary problems are available. The field velocity method (Parameswaran and Baeder, [10], Singh and Baeder, [11] and [12], Sitaraman et al. [13], Zhan and Qian, [14] and [15]), which adopts the grid speed technique to simulate the velocity change of the flow field, has been applied successfully to calculate the gust response of the airfoil/wing (Harish and Alex [16]; Raveh; Raveh et al., [17] and [18], Yang et al., [19]). This method has shown to be suitable for computation of step change of airfoil. The method of conventional field velocity is usually used to calculate the indicial response by incorporating unsteady flow conditions via grid movement in CFD simulations (Parameswaran and Baeder, [20] (Singh and Baeder, [21])). The main privilege of this method is direct calculation of aerodynamic responses to step changes in flow conditions. An impulsive change in the angle-of-attack can be considered as an impulsive superposition of a uniform velocity field to the free stream. The magnitude of the indicial change for the angle of attack is used for calculation of the magnitude of normal velocity. In this method, the necessity of uniform distribution of time step over the entire flow domain is guaranteed. In addition, the airfoil is not made to pitch. Hence, the influence of pure angle-of-attack and pitch rate are decoupled efficiently. A similar methodology for simulating responses of an airfoil to step changes in pitch rate and interaction with vertical gusts exists. Moreover, the field velocity method is also applied for prediction of the effects of the trailed vortex wake from the other rotor blades in helicopters, compressors or other turbo machineries. A time dependence study illustrates that a smooth and accurate solution in time requires the consistent evaluation of time metrics in order to satisfy the geometric constitutive law (Sitaraman et al., [22]).

The objective of the present work is to compute unsteady transonic inviscid and viscous flow fields over a pitching NACA0012 airfoil at various angles of the attack. A pressure based implicit procedure to solve the Euler and Navier-Stokes equations is developed to predict flows around the pitching airfoil with high resolution scheme. In this process, nonorthogonal and non moving mesh with collocated finite volume formulation are used. In order to simulate plunging airfoil, oscillation of flow boundary condition is applied. The boundedness criteria for this procedure are determined from

M.H. Djavareshkian Associate Prof.  
Ferdowsi University of Mashhad  
IRAN

A.R. Faghihi MSc Student  
Ferdowsi University of Mashhad  
IRAN

Normalized Variable Diagram (NVD) scheme. The procedure incorporates the  $k-\epsilon$  eddy-viscosity turbulence model. The algorithm is tested for inviscid and turbulent transonic aerodynamic flows around plunging airfoil. The results are compared with other existing numerical solutions and with experiment data. The comparisons show that the resolution quality of the developed algorithm is considerable.

## II. Governing equations and discretization

The basic equations, which describe conservation of mass, momentum and scalar quantities, can be expressed in Cartesian tensor form as:

$$\frac{\partial}{\partial t}(\rho) + \frac{\partial}{\partial x_i}(\rho u_i) = 0 \quad (1)$$

$$\frac{\partial}{\partial t}(\rho u_i) + \frac{\partial}{\partial x_j}(\rho u_i u_j - T_{ij}) = S_i'' \quad (2)$$

$$\frac{\partial}{\partial t}(\rho \phi) + \frac{\partial}{\partial x_i}(\rho u_i \phi - q_i) = S^\phi \quad (3)$$

The stress tensor and scalar flux vector are usually expressed in terms of basic dependent variable. The stress tensor for a Newtonian fluid is

$$T_{ij} = -\left(P + \frac{2}{3}\mu \frac{\partial u_k}{\partial x_k}\right)\delta_{ij} + \mu\left(\frac{\partial u_i}{\partial x_j} + \frac{\partial u_j}{\partial x_i}\right) \quad (4)$$

The scalar flux vector usually given by the Fourier-type law is

$$q_i = \Gamma_\phi \left(\frac{\partial \phi}{\partial x_i}\right) \quad (5)$$

Turbulence is accounted for by adopting  $k-\epsilon$  turbulence model. The governing equations for these quantities are

$$\frac{\partial}{\partial t}(\rho k) + \frac{\partial}{\partial x_i}(\rho u_i k - \Gamma_k \frac{\partial k}{\partial x_i}) = G - \rho \epsilon + D_{comp} + \Theta_{diff} \quad (6)$$

$$\frac{\partial}{\partial t}(\rho \epsilon) + \frac{\partial}{\partial x_i}(\rho u_i \epsilon - \Gamma_\epsilon \frac{\partial \epsilon}{\partial x_i}) = +C_{1\epsilon} \frac{\epsilon}{\kappa} G - C_{2\epsilon} \rho \frac{\epsilon^2}{\kappa} \quad (7)$$

The turbulent viscosity and diffusivity coefficients are defined by

$$\mu_t = C_\mu \rho \frac{k^2}{\epsilon} \quad (8)$$

$$\Gamma_\phi = \left(\frac{\mu_t}{\sigma_\phi}\right) \quad (9)$$

and the generation term G in eqs. (6) and (7) is defined by

$$G = \mu_t \left( \left[ \frac{\partial U_i}{\partial x_j} + \frac{\partial U_j}{\partial x_i} \right] \frac{\partial U_i}{\partial x_j} - \frac{2}{3} \delta_{ij} \left[ \frac{\partial U_l}{\partial x_l} + \rho k \right] \frac{\partial U_l}{\partial x_i} \right) \quad (10)$$

The term  $D_{comp}$  and  $\Theta_{diff}$  are additional contributions to the standard  $k-\epsilon$  model often introduced to account for the effects of compressibility. In this work, the models proposed by (Yang et al., [23]). are adopted, namely,

$$D_{comp} = -\frac{9}{55} \rho k \frac{\partial u_i}{\partial x_i} - \frac{1}{\rho} \cdot \frac{\mu_t}{\rho} \cdot \frac{\partial \rho}{\partial x_i} \frac{\partial p}{\partial x_i} \quad (11)$$

$$\Theta_{diff} = 0 \quad (12)$$

The latter being appropriate for high Reynolds number flows, as it is the case here. The values of the turbulence model coefficients used in the present work are given in

Table 2(Yang et al., [23]).

The discretization of the above differential equations is carried out using a finite-volume approach. First, the solution domain is divided into a finite number of discrete volumes or cells, where all variables are stored at their geometric centers (see e.g. Fig. 1). The equations are then integrated over all the control volumes by using the Gaussian theorem. The development of the discrete expressions to be presented is effected with reference to only one face of the control volume, namely,  $e$ , for the sake of brevity.

For any variable  $\phi$  (which may now also stand for the velocity components), the result of the integration yields

$$\frac{\delta V}{\delta t} [(\rho \phi)_p^{n+1} - (\rho \phi)_p^n] + I_e - I_w + I_n - I_s = S_\phi \delta V \quad (13)$$

Where  $I_{(s)}$  are the combined cell-face convection  $I^c$  and diffusion  $I^D$  fluxes. The diffusion flux is approximated by central differences and can be written for cell-face  $e$  of the control volume in Fig.1 as an example as:

$$I_e^D = D_e (\phi_p - \phi_e) - S_e^\phi \quad (14)$$

Where  $S_e^\phi$  stands for cross derivative arising from mesh nonorthogonality. The discretization of the convective flux, however, requires special attention and is the subject of the various schemes developed. A representation of the convective flux for cell-face  $e$  is:

$$I_e^c = (\rho V A)_e \phi_e = F_e \phi_e \quad (15)$$

The value of the dependent variable  $\phi_e$  is not known and should be estimated using an interpolation procedure, from the values at neighboring grid points.  $\phi_e$  is determined by the SBIC scheme(Djavareshkian [24]), that it is based on the NVD technique, used for interpolation from the nodes E, P and W. The expression can be written as

$$\phi_e = \phi_W + (\phi_E - \phi_W) \cdot \tilde{\phi}_e \quad (16)$$

The functional relationship used in SBIC scheme for  $\tilde{\phi}_e$  is given by:

$$\tilde{\phi}_e = \tilde{\phi}_P \quad \text{if} \quad \tilde{\phi}_P \notin [0,1]$$

$$\tilde{\phi}_e = -\frac{\tilde{x}_P - \tilde{x}_e}{K(\tilde{x}_P - 1)} \tilde{\phi}_P^2 + \left(1 + \frac{\tilde{x}_P - \tilde{x}_e}{K(\tilde{x}_P - 1)}\right) \tilde{\phi}_P \quad \text{if} \quad \tilde{\phi}_P \in [0, K] \quad (17)$$

$$\tilde{\phi}_e = \frac{\tilde{x}_P - \tilde{x}_e}{\tilde{x}_P - 1} + \frac{\tilde{x}_e - 1}{\tilde{x}_P - 1} \tilde{\phi}_P \quad \text{if} \quad \tilde{\phi}_P \in [K, 1]$$

$$0 \leq K \leq 0.5$$

where

$$\tilde{\phi}_P = \frac{\phi_P - \phi_W}{\phi_E - \phi_W} \quad \tilde{\phi}_e = \frac{\phi_e - \phi_W}{\phi_E - \phi_W} \quad (18)$$

$$\tilde{x}_e = \frac{x_e - x_W}{x_E - x_W} \quad \tilde{x}_P = \frac{x_P - x_W}{x_E - x_W}$$

The limits on the select each value of  $K$  could be determined in the following way. Obviously the lower limit is to keep  $K=0$ , which would represent switching between upwind and central differencing. This should not be favored because; it is essential to avoid the abrupt switching between the schemes in order to achieve the converged solution. The upper limit of  $K$  is 0.5, since it represents the constant gradient and there is no need to use anything else than central differencing in that case. The value of  $K$  should be kept as low as possible in order to achieve the maximum resolution of the scheme.

According to Eq. (17), if  $\tilde{\phi}_P$  (or  $\tilde{\phi}_C$  normalized variable at the central node) does not belong to  $[0,1]$ , the space discretization is first order, otherwise the SBIC scheme has second order accuracy from point of view space discretization. The details of how the interpolation is made is dealt with ([24]); it suffices to say that the discretized equations resulting from each approximations take the form:

$$A_P \cdot \phi_P = \sum_{m=E,W,N,S} A_m \cdot \phi_m + S'_\phi \quad (19)$$

Where  $A_{(s)}$  are the convection-diffusion coefficients. The term  $S'_\phi$  in Eq.0 contains quantities arising from non-orthogonality, numerical dissipation terms, external sources, deferred correction terms, and  $(\rho \delta v / \delta t) \phi_P$  of the old time-step/iteration level. For the momentum equations it is easy to separate out the pressure-gradient source from the convected momentum fluxes.

### III. Solution Algorithm

Most contemporary pressure-based methods employ a sequential iteration technique in which the different conservation equations are solved one after another. The common approach taken in enforcing continuity is by combining the equation for continuity with those of momentum to derive an equation for pressure or pressure-correction. The PISO [25] algorithm is used in this work.

### IV. New Time Advancement Algorithm

In this research, the new time advancement algorithm, is utilized an internal and external loop for calculation (Fig 2).

### V. Boundary Conditions

At the inlet of the domain, only three of the four variables need to be prescribed: the total temperature, the angle of attack, and the total pressure. The pressure is obtained by zeroth order extrapolation from interior points. At outlet, the pressure is fixed. Slip boundary conditions are used on the lower and upper walls. In the case of viscous flow, the non-slip condition is applied at the airfoil surfaces. To account for the steep variations in turbulent boundary layers near solid walls, wall functions, which define the velocity profile in the vicinity of no-slip boundaries, are employed.

### VI. Results and discussion

In this section, the results of the viscous flows over a plunging NACA0012 airfoil are indicated. The simulations are performed at a higher Reynolds number. In particular, we aim to validate the simulation with existing numerical results of a plunging airfoil, and study the lift characteristics of a plunging airfoil. The steady state solutions at  $1^\circ$  angle of attack are used as initial conditions for time-marching calculations. **Error! Reference source not found.** provides an illustration of pure-plunge motion for an airfoil with a free stream Mach number of 0.8 and angle of attack  $1^\circ$ . The parameters of motion and flow field are described in Table 1. The heaving velocity of the sinusoidal plunging motion is given as:

$$v_o(t) = -M_\infty \cdot \sin\left(\frac{\pi}{180}\right) \cdot \sin(\omega(t - \Delta t)) \quad (20)$$

$$v_o(t) = \frac{\dot{h}(t)}{a_\infty} \quad (21)$$

$$\Delta t = \frac{L}{U_\infty} \quad (22)$$

The significant point in simulation heaving airfoil with oscillation boundary condition considers a lag phase ( $\Delta t$ ). Eq.18 has been non-dimensionalized by the free stream speed of sound  $a_\infty$ . The free stream velocities for unsteady computations are set to  $u_{inlet} = U_\infty$  and  $v_{inlet} = u_\infty \sin(\alpha(t))$ . A H-type mesh is generated to model the airfoil and the surrounding flow. The schematic of this grid which used in the present simulation is shown in Fig. 4. The grid dependence test for Navier-Stokes Equation on the NACA0012 airfoil at  $M_\infty = 0.8$ ,  $\alpha = 1^\circ$  is indicated in Fig.5. Three different mesh sizes were considered: 27680, 57950 and 115960 cells and

each simulation emerged from its fully converged solution. These comparisons show that the solutions using oscillating boundary condition method has good prediction.

The computed variation of the lift coefficient versus angle of attack for viscous flows during the third cycle is compared with that Lin [26] and Uzun [27] and in **Error! Reference source not found.** For presented viscous case, the turbulence quantities were specified at inlet to correspond to 0.008 turbulence intensity and a dissipation length scale of 10% of the airfoil chord. The value of  $K$  in SBIC scheme for the case of validation in fig. 6 is 0.05. Fig. 6 shows the computed variation of lift coefficient versus angle of attack for viscous case which is in close agreement with published results. Uzun [27] used dynamic mesh with a parallel algorithm for the solution of unsteady Euler equation on unstructured reformatting grids while in this study non moving mesh with oscillation of flow boundary condition is applied. Lin used multi reference frame for simulation of heaving motions. This comparison shows the resolution of these methods is considerable. But the present method is simple and has low cost for calculation, on the other hand, the dynamic mesh and multi references of frame method are time consuming and very complicated to development. Table 3 indicates CPU Time comparison for different algorithms. The numbers of iteration to satisfy convergence criteria for the external loops of algorithms (a),(b) and (c) are approximately 500,0 and 2-3 respectively and for internal loops of these algorithms are about 0, 20-30 and 3-5 respectively. As a result, the two algorithms (a) and (b) are time consuming and CPU time for new method is considerably decreased.

## VII. Conclusions

A pressure based implicit procedure to solve the Euler and Navier-Stokes equations is developed to predict transonic viscous and inviscid flows around the plunging airfoil with high resolution scheme. In order to simulate pitching airfoil, oscillation of flow boundary condition is applied. The boundedness criteria for this procedure are determined from Normalized Variable Diagram (NVD) scheme. The main findings can be summarized as follows: 1- The plunging airfoil simulation with the oscillation of flow boundary condition with fix grid is very simple and has low cost. 2-The grid dependence test with high resolution scheme indicates that an acceptable solution can be obtained even on fairly coarse 3-the agreement between numerical and experimental data is considerable. 4-The CPU time for new method considerably reduce.

## References

- [1] Shankar, V., Ide, H., 1988, Aeroelastic computations of flexible configurations, Computers & Structures 30, 15-28.
- [2] Goswami, A., Parpia, I.H., 1991, Grid Restructuring for Moving Boundaries, AIAA-91-1589-CP.
- [3] Batina, J.T., 1990. Unsteady Euler airfoil solutions using unstructured dynamic meshes. AIAA Journal 28, 1381-1388.
- [4] Zheng, Y., Lewis, R.W., Gethin, D.T., 1996, Three-dimensional unstructured mesh generation: Part 1, Fundamental aspects of triangulation and point creation, Computer Methods in Applied Mechanics and Engineering 134, 249-268.
- [5] Nakahashi, K., Deiwert, G.S., 1987, Self-adaptive-grid method with application to airfoil flow. AIAA Journal 25, 513-520.
- [6] Levine, M., Williams, M., Whitlow, W., 1988. Body Conforming Grids for General Unsteady Airfoil Motion, Structures, Structural Dynamics and Materials Conference; 29th, Williamsburg, VA; United States pp. 530-540.
- [7] Guruswamy, G.P., 1990, Unsteady aerodynamic and aeroelastic calculations for wings using Euler equations. AIAA Journal 28, 461-469.
- [8] Lohner, R., 1988, An adaptive finite element solver for transient problems with moving bodies, Computers & Structures 30, 303-317.
- [9] Farhat, C., Lin, T.Y., 1990, Transient Aeroelastic Computations Using Multiple Moving Frames of Reference. AIAA Journal, 953-965.
- [10] Parameswaran, V., Baeder, J.D., 1997, Indicial aerodynamics in compressible flow-direct computational fluid dynamic calculations. American Institute of Aeronautics and Astronautics, Reston, VA, ETATS-UNIS.
- [11] Singh, R. and Baeder, J., 1963, Transonic effects on acoustics of blade-vortex interaction, Archive Set 748, American Institute of Aeronautics and Astronautics.
- [12] Singh, R., Baeder, J.D., 1997, Direct calculation of three-dimensional indicial lift response using computational fluid dynamics, American Institute of Aeronautics and Astronautics, Reston, VA, ETATS-UNIS.
- [13] Sitaraman, J., Baeder, J. and Iyengar, V., 2003, On the Field Velocity Approach and Geometric Conservation Law for Unsteady Flow Simulations, 16th AIAA Computational Fluid Dynamics Conference, American Institute of Aeronautics and Astronautics.
- [14] Zhan, H., Qian, W.-q., 2007, Numerical simulation of gust response for airfoil and wing, Acta, Aerodynamic, Sinica 25, 531-536.
- [15] Zhan, H., Qian, W.-q., 2009, Numerical simulation on gust response of elastic wing, Chinese Journal of Computational Mechanics 26, 270-275.
- [16] Harish, G., Alex, P., 2008. A Numerical Study of Gust Suppression by Flapping Airfoils, 26th AIAA Applied Aerodynamics Conference.
- [17] Raveh, D.E., Gust-Response Analysis of Free Elastic Aircraft in the Transonic Flight Regime. Journal of Aircraft 48, 1204-1211.
- [18] Raveh, D.E., Liu, D.D., Strganac, T.W., Dowell, E.H., Silva, W.A., Beran, P.S., 2007. CFD-Based Models of Aerodynamic Gust Response. Journal of Aircraft 44, 888-897.
- [19] Yang, G., Obayashi, S., Guruswamy, G.P., 2004. Numerical Analyses of Discrete Gust Response for an Aircraft. Journal of Aircraft 41, 1353-1359.
- [20] Parameswaran, V., Baeder, J.D., 1997. Indicial aerodynamics in compressible flow-direct computational fluid dynamic calculations. American Institute of Aeronautics and Astronautics, Reston, VA, ETATS-UNIS.
- [21] Singh, R., Baeder, J.D., 1997. Direct calculation of three-dimensional indicial lift response using computational fluid dynamics. American Institute of Aeronautics and Astronautics, Reston, VA, ETATS-UNIS.
- [22] Sitaraman, J., Baeder, J., Iyengar, V., 2003. On the Field Velocity Approach and Geometric Conservation Law for Unsteady Flow Simulations, 16th AIAA Computational Fluid Dynamics Conference. American Institute of Aeronautics and Astronautics.
- [23] Yang, Z.Y., Chin, S.B., Swithenbank, J., 1991. On the Modeling of the k-equation for Compressible flow., 7th International Symposium on numerical methods in laminar and turbulent flow, Stanford, CA.
- [24] Djavareshkian, M.H. Pressure-based compressible calculation method utilizing normalized variable diagram schmen, Iranian Journal of Science and Technology, Volume 28, Number B4, 2004, pp.495-500
- [25] Issa, R.I., 1986. Solution of the implicitly discretised fluid flow equations by operator-splitting. Journal of Computational Physics 62, 40-65.
- [26] Lin, T.Y. 1990. A Multiple Frames of Reference Approach to Aeroelastic Computations: Application to Airfoil Flutter Analysis. University of Colorado
- [27] Uzun, A. 1999, Parallel Computations Of Unsteady Euler Equations On Dynamically Deforming Unstructured Grid. Msc Thesis, Purdue University

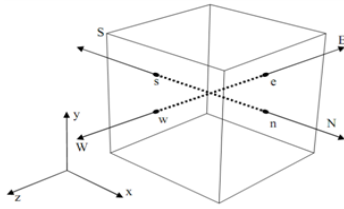


Fig.1. Finite volume and storage arrangement

Table 1 Pure plunging motion parameters

|          |            |     |
|----------|------------|-----|
| $\kappa$ | $M_\infty$ | $c$ |
| 0.2      | 0.8        | 1.0 |

Table 2 Values of empirical coefficients in the standard k- $\epsilon$  turbulence model

|       |       |         |            |                   |
|-------|-------|---------|------------|-------------------|
| $C_1$ | $C_2$ | $C_\mu$ | $\sigma_k$ | $\sigma_\epsilon$ |
| 1.44  | 1.92  | 0.09    | 1.0        | 1.3               |

Table 3. CPU Time comparison for different algorithms

|                   | Iterative Algorithm | Non-Iterative Algorithm | New Algorithm |
|-------------------|---------------------|-------------------------|---------------|
| Internal Loop No. | -                   | 20-30                   | 3-5           |
| External Loop No. | 500                 | -                       | 2-3           |
| CPU Time (min)    | 5000                | 2000                    | 180           |

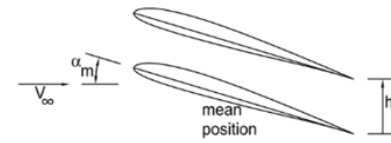


Figure 2 Pure Plunge Motion definition,  $\alpha_m=1^\circ$

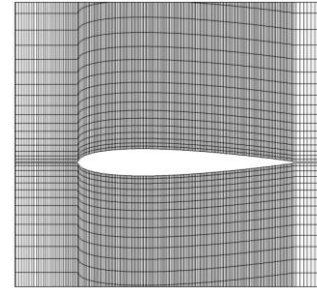


Fig.4. Part of the H Grid

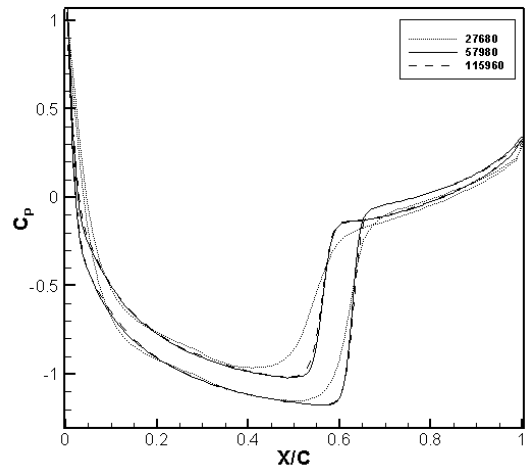


Figure 3 Grid dependency results for NACA0012,  $M_\infty=0.8$ ,  $\alpha=1^\circ$

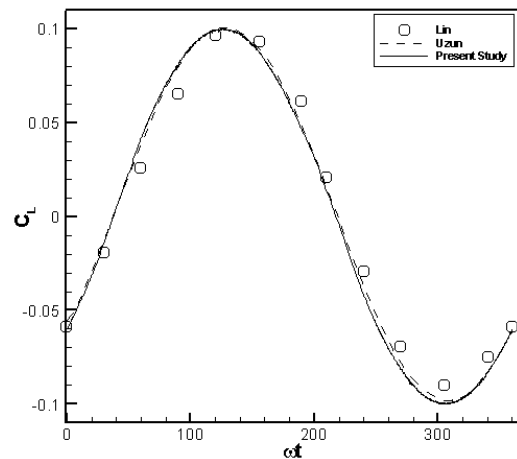


Figure 6 Lift coefficient distribution for Pure Plunging Motion,  $M=0.8$ ,  $\kappa=0.2$ , :NACA0012

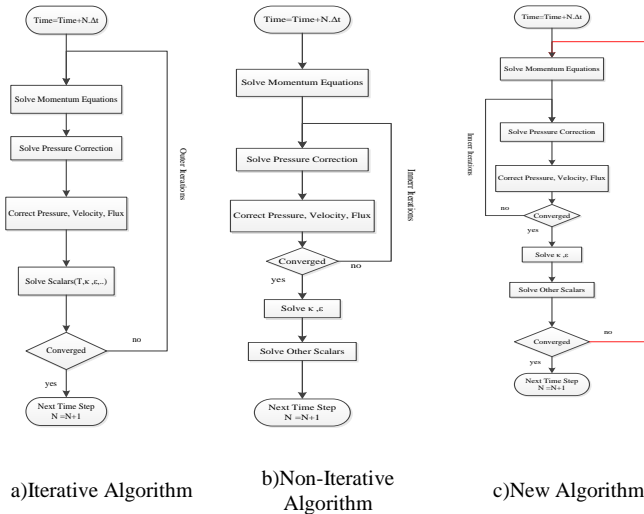


Fig. 2 Different Flowcharts for Time advancement